Contents lists available at ScienceDirect

Extreme Mechanics Letters

journal homepage: www.elsevier.com/locate/eml



Confocal microscopy observations of electrical pre-breakdown of bi-layer elastomer dielectrics



Pavida Charoen-Rajapark, David R. Clarke*

School of Engineering and Applied Sciences, Harvard University, Boston, MA 02134, United States of America

ARTICLE INFO

Article history: Received 29 June 2021 Received in revised form 18 August 2021 Accepted 19 August 2021 Available online 30 August 2021

Keywords:
Electrical breakdown
Confocal microscopy
Surface instability
Elastomers
Geometrical phase transition

ABSTRACT

At high electric fields, the electrical energy stored in a soft elastomer dielectric can be comparable to the mechanical deformation energy it produces. This has led to the development of a class of electrically controlled, large strain dielectric elastomer actuators for soft robotics and energy harvesting devices. At large electric fields, the electro-mechanically induced deformation can lead to pseudo-periodic surface morphological instabilities which then grow with increasing field into stable pre-breakdown defects prior to final, irreversible electrical breakdown. Under these extremes of combined large electrical and mechanical deformations, the morphological evolution of the pre-breakdown defects has not hitherto been reported. In contrast to the filamentary breakdown of much stiffer dielectrics, fluorescence confocal microscopy reveals an array of defects that evolve through a complex, reversible series of morphologies, transitioning from axi-symmetric "pits" to "crack-like" shapes that can "twist" and deflect, and finally open to form an array of holes. The observations suggest that the transitions, from axi-symmetric pits to flat, slit-like defects and then to an array of holes, are geometric instabilities. The implications for using a soft elastomer layer to increase the dielectric breakdown of a stiffer dielectric are discussed.

© 2021 Elsevier Ltd. All rights reserved.

1. Introduction

Most dielectrics (including semiconductors) in which electrical breakdown has been investigated are materials having a high elastic modulus (several GPa to hundreds of GPa) and consequently the mechanical deformation associated with high electric fields (>1 V/micron) are likely to be small. This is because the electrical energy per unit volume scales with electric field, E, as E^2 whereas elastic strain energy density scales with elastic strain, e, as μ e^2 . ε and μ are the dielectric constant and elastic modulus, respectively. Comparison of these energies suggest that they are comparable and result in significant strains at normalized electric fields, Ω , given by [1–4]:

$$\Omega = \sqrt{\varepsilon/\mu} \frac{V_o}{h} \gg 0$$

where V_0 and h are the applied voltage and elastomer thickness, respectively. With the increasing use of soft elastomers ($\mu \sim 0.1$ –10 MPa) under large electric fields (>10 V/micron) in the development of a variety of dielectric elastomer actuators and energy harvesting devices, these dielectrics are being used under conditions where the elastic and electrostatic energies are comparable. One manifestation of this is that an initially flat surface of

a soft dielectric is unstable to morphological perturbations above a critical electric field and a pseudo-periodic array of pits forms. The pits are visible to the eye, as well as by optical microscopy, and have average spacing that depends on the thickness of the soft elastomer [5,6]. (A video recording of the pitting, observed in reflected light optical microscopy, with increasing and then decreasing electric field is included in the Supplementary Materials). The instability has been extensively analyzed [1,3,7,8]. As the electric field is increased beyond this instability condition, the pits extend deeper into the elastomer and above an even higher electric field, catastrophic electrical breakdown occurs. If electrical breakdown does not occur and the field is reduced, the pitting phenomenon is reversible. This forms the basis for a reversible, privacy window [5,9] as the pits scatter light and the optical transmittance of the elastomer can be controlled over a wide range of values by controlling the applied voltage [6]. In contrast to the electro-mechanical analyzes which predict a bifurcation instability [3], the pits form by a nucleation and growth process. Although studies of the optical scattering by the pits have been reported, they are neither precise enough nor sufficiently interpretable to provide insight into the mechanisms by which the pits extend post-instability into the elastomer. Furthermore, microscopy studies have been unable to reveal the shape evolution once the surface becomes steep, as illustrated by the confocal image in Fig. 1(a), possibly because of large optical refraction effects and low contrast. Consequently, the defects well below the

^{*} Corresponding author. E-mail address: clarke@seas.harvard.edu (D.R. Clarke).

macroscopic surface of the elastomer cannot be resolved. As will be described in this work, using fluorescence confocal microscopy to enhance contrast, the pit evolution consists of a series of large strain and complex morphological changes until, ideally, an array of hyperbolic funnels form penetrating through the elastomer. At each step, the morphological instabilities are reversible when the electric field is subsequently decreased unless permanent breakdown occurs. The observed behavior is quite distinct from the usual filamentary pre-breakdown that occurs in stiff materials and has implications for dielectric breakdown in elastomers.

The observations reported in this work are made in a configuration consisting of two dielectric elastomer layers, one significantly softer than the other, deposited on an ITO coated glass substrate with a compliant CNT mat network on top of the softer dielectric. To enhance contrast in the otherwise transparent elastomers, they were each dyed with a fluorescent dye. Fig. 1(b). This is the same structure used in previous experiments relating optical transmittance to the electric-field induced surface morphological instability of a soft elastomer [5,9]. Following the work of Wang et al. [1], the bi-layer elastomer configuration was selected because the electrical field induced surface instabilities in the soft elastomer, once formed, growing stably with increasing electric field and do not lead to irreversible, catastrophic breakdown, until the electric field approaches the breakdown field of the stiffer elastomer layer. The rationale for using a stiffer elastomer layer is to raise the voltage at which catastrophic breakdown of the bilayer occurs since the dielectric breakdown field of an elastomer generally increases with its elastic modulus [1]. In turn, this enables the electric field in the softer elastomer to be varied at fields below which complete failure occurs. In the experiments reported here, a voltage between the ITO electrode and the CNT network was applied in discrete steps and observations were recorded by confocal optical imaging at successively higher voltages.

2. Materials and methods

All the devices studied comprised a layer of 10:1 mixing ratio of base to cross-linker of silicone elastomer (Sylgard 184, Dow Corning) on an ITO coated glass substrate with a layer of 50:1 Sylgard 184 on top, unless otherwise stated. (The ITO coated glass had a thickness 150 um, and a 30-60 Ohm resistivity, and was purchased from SPI Supplies). According to the literature, the elastic shear modulus of the 10:1 and 50:1 composition, are 700 kPa and 3 kPa [10,11], respectively. The dielectric constant for 10:1 Sylgard 184 is reported to be 2.65 [12]. For ease of distinguishing the two layers in the confocal microscope, the stiffer 10:1 elastomer was dyed with an alkyne purple fluorescence dye (BDP 558/568 alkyne, Lumiprobe Corporation) and the softer elastomer with a different alkyne green fluorescence dye (BDP FL alkyne, Lumiprobe Corporation). The elastomers were deposited by spin-coating. After the stiff layer was deposited it was cured at 70 °C for 24 h before the soft layer was deposited and then also thermally cured at the same temperature and time. Unless otherwise stated, the thicknesses of the soft and stiff elastomers were 50 and 30 µm thick, respectively. A CNT electrode (P3-SWNT, Carbon Solutions, Inc.) was transferred by stamping onto the surface of the cured soft elastomer using a Teflon filter (100 nm pore size and 47 mm diameter, Omnipore). The CNT electrode was deposited as described in the appendix of Ref. [2].

The observations were performed in air and the structure was mounted so that the CNT surface faced away from the objective lens of the microscope. This configuration was chosen to minimize artifacts associated with varying refraction angles from local variations in surface orientation affecting the incident illumination intensity.

The confocal microscopy observations were recorded using a confocal microscope (Model 710, Zeiss) with a 20x, NA 0.8, objective lens (Plan-Apochromat, Zeiss). This enabled a stack of images. $320 \times 320 \, \mu m$ in width, with a slice thickness of 0.91 μm , to be recorded as a series of images at each voltage. The number of voxels in a single image was 512 \times 512. Voltages were applied using a high-voltage power supply (Model 610E, Trek, Inc.). The device and all the electrical leads were mounted on a rubber sheet to insulate the device and the ground. Although the voltages used were relatively high, current limiters were used to ensure that the current was always substantially lower than 2 mA. The confocal images, such as Fig. 1(c) and subsequent images, were formed by combining the output of two photomultiplier detectors, one to capture the fluorescence of the green dye excited by the 488 nm laser and the other the purple dye excited by the 555 nm laser, under the control of the microscope's Zeiss Zen software. Subsequent image manipulations were performed using a MATLAB program. Typically, the acquisition time for a stack of 110 images was 2 min so rapid changes in the defect shape could not be recorded but rather a sequence of images recorded following stepwise changes in voltage.

To gain additional information about the defect shape evolution, the confocal images were also visualized by constructing, using MATLAB, images of the soft elastomer surface at different electric fields. This enables a 3D reconstruction of the elastomer surface as a series of contours, spaced 0.91 μm apart, from the individual image slices. For clarity, these images are inverted. Although the precise dimensions of the defects in the confocal images are sensitive to the image threshold used to define the surface, the complex nature of the microstructural evolution becomes more evident.

3. Confocal microscopy observations

Before any voltage is applied to the bilayer elastomer structure, the surface of the soft elastomer, as well as its interface with the stiffer elastomer, are flat and smooth. Fig. 1(c). Sequences of confocal images indicate that the two interfaces remained planar with increasing voltage until circular depressions ("pits") nucleate randomly at the CNT coated surface over a narrow range of voltage. The initial, electric field induced surface morphological instability shape is consistent with previously reported experiments by Wang et al. [1] and Kjeer et al. [6] as well as the predictions of elastic-electrostatic perturbation bifurcation models [3] and with instability models [1,13]. They take the form of a pseudo-periodic array of funnel shaped pits that nucleate at the surface of the elastomer. Consistent with some of the earlier reports [6,14], the pits form at the elastomer surface by a nucleation and growth process as the electric field is increased and adopt an average in-plane spacing that remains fixed with further voltage increases. Then, once formed, they adopt an approximately hexagonal arrangement and no new pits subsequently form. The average spacing between pits is dependent on the thickness of the soft dielectric [1,14]. During the formation of pits at this initial instability, the interface between the soft and hard elastomers remains flat.

With further increase in voltage a complex evolution in shape of the pre-breakdown defects occurs. The main features are illustrated with the confocal image stack in Fig. 2 recorded at 5.4 kV. In these image stacks, each individual image is a cross-section of the elastomer at the depth corresponding to the location in the stack. So, each stack captures the defect at the voltage indicated. The images indicate that as the nucleated pits extend deeper into the soft elastomer, their pit shape transitions into flat, slit-like features, superficially like cracks or creases, as seen in slices 90 to 69 in Fig. 2.

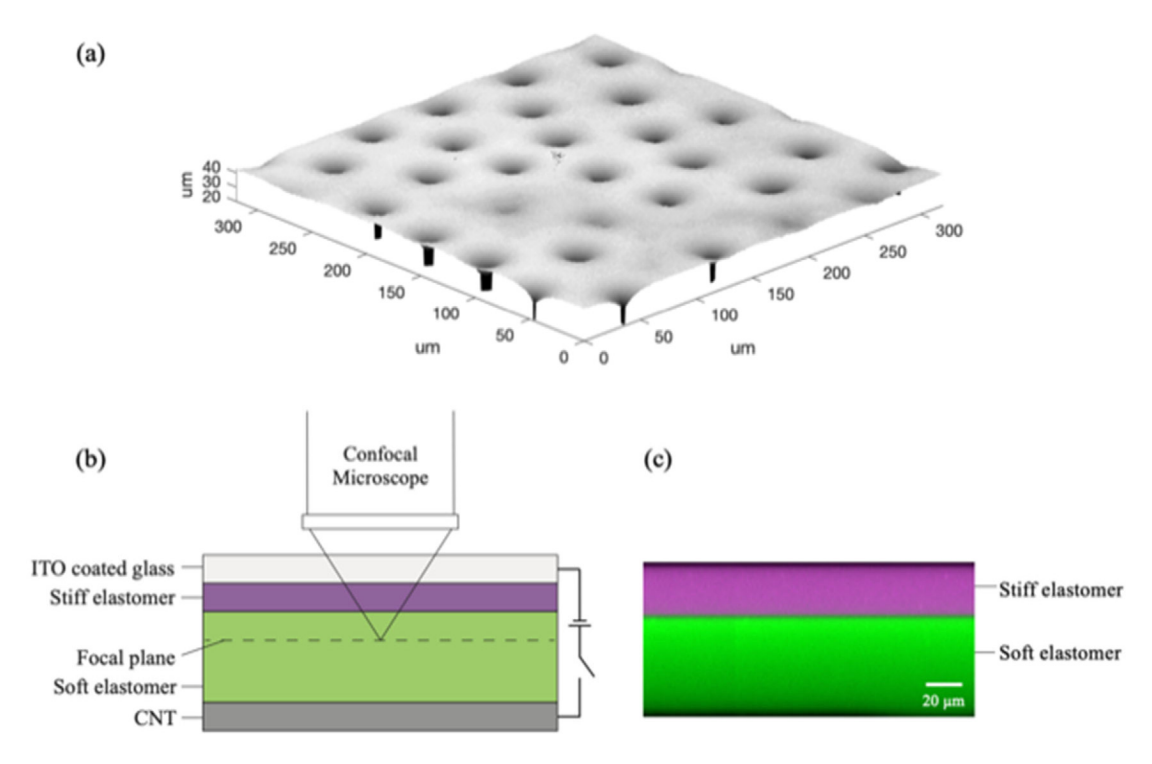


Fig. 1. (a) Perspective view of the surface of the soft elastomer, without any dye, at a voltage of 4.5 kV illustrating an array of electric-field induced pits. The contrast reveals the surface curvature around each pit but no information, except for the signal spikes, well below the surface. (b) schematic of the confocal imaging used to record the images of the dyed elastomers presented in this work. To minimize spatial variations that can cause refractive effects in the illumination, the sample is viewed through the ITO coated glass. (c) Cross-section recorded using fluorescence imaging with the stiffer elastomer dyed purple and the softer elastomer dyed green. The dyes were used to enhance image contrast. The CNT electrode and glass are not visible in the fluorescence images.

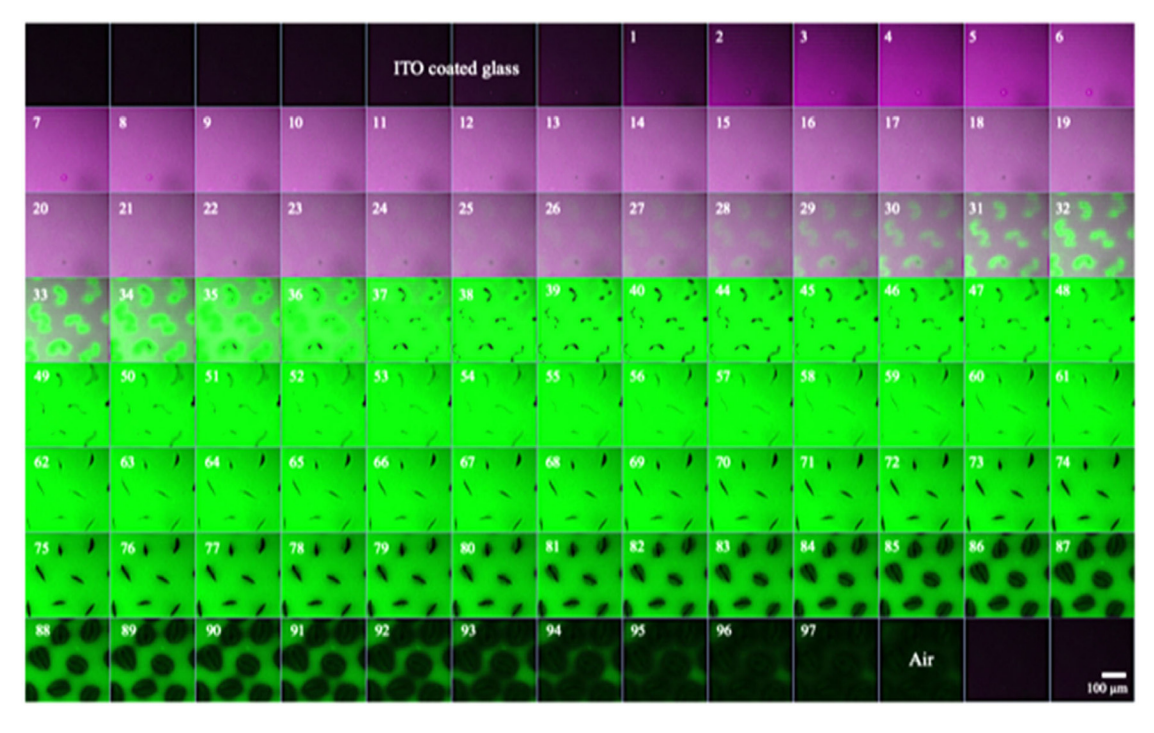


Fig. 2. Fluorescence confocal image stack through the thickness of the bilayer elastomer from the glass (top left) to the air (bottom right) recorded at a voltage of 5.4 kV. The spacing between the images in the stack is 0.91 μm.

The defects appear dark because reduced fluorescence intensity reaches the confocal microscope detector either because a significant fraction of the incident illumination, or the stimulated fluorescence, is refracted or scattered away by the defect. It is not possible to determine whether these features are "cracks" or

"creases" since we cannot determine their width. For this reason, they will simply be referred to in the following as "slit-like" features.

With increasing voltage, they extend deeper into the soft elastomer and many of them subsequently also adopt a twisted

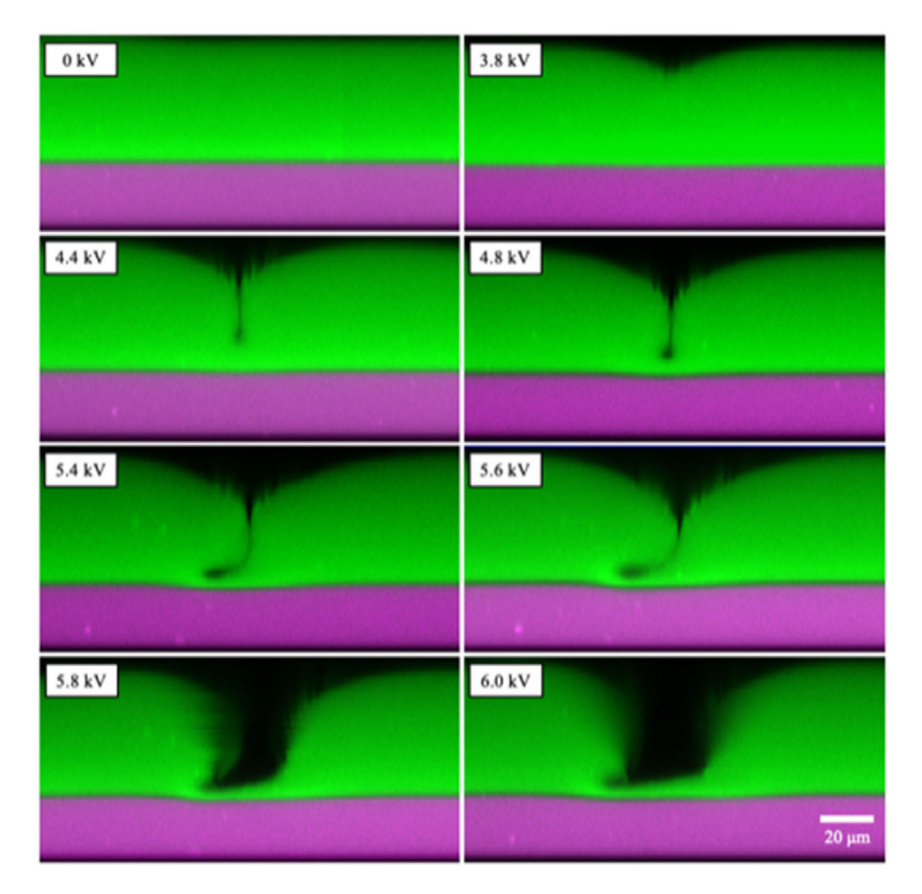


Fig. 3. Cross-sectional images of the same defect recorded at successively higher voltages illustrating the post-instability shape evolution with increasing electric field

"S-shape" or "C" configuration in individual images, as seen in slice 56 to 40. At higher voltages still, the defects, propagating in the nominal electric field direction, deflect and extend parallel to the interface between the soft and stiff elastomers. This is not clear in the sequence of images slices, such as those in Fig. 2, but can be readily observed in cross-sections through the stack, such as in Fig. 3. It is evident from these observations that the deflected defects remain within the soft elastomer layer and do not propagate along the soft/stiff elastomer interface. Concurrently the interface is locally displaced towards the lower, ITO glass electrode as if the softer (green) material adjoining the deflected crack pushes into the stiffer (purple) elastomer. This can be discerned in the slices 28 to 33 of Fig. 2. The interface between the soft and stiff elastomers remains planar until the defect is close to the interface.

Complementary surface contour images, such as Fig. 4(a), indicate that the transition from a three-dimensional pit to the planar shape, seen in cross-section in Fig. 3, for instance, is abrupt. These images also reveal the variety of contorted shapes occurring even within a short distance. The next stage in the defect evolution as the voltage is increased is that the deflected defect open to form a flat-bottomed hole in the soft elastomer, as illustrated in both the cross-sectional images and the surface contour plot of Fig. 4(b). The cross-sectional shape of the hole can be quite irregular and vary from one to another but in every case has an approximately flat surface parallel to the original soft/stiff elastomer interface. The images capture a variety of these shapes, some in the form of mesas until, presumably, forming an array of holes. It should be emphasized that this last stage in the evolution of the prebreakdown defect shape was not always observed since electrical breakdown typically occurred somewhere else in the sample not under observation.

When a thinner soft elastomer layer is used, the same defect evolution occurs with increasing voltage except that the kinking transition is not always observed. As illustrated in Fig. 5, there is considerable deformation of the initially flat, stiff elastomer and the slit-like defects open laterally. In this example, the electric field at which the defects open is $\sim 110 \text{ V/micron}$.

Lastly, and significantly, if electrical breakdown does not occur during the extension of the pre-breakdown defects and the voltage is then decreased the growth sequence reverses as illustrated by the two sequences shown in Fig. 6. The precise voltage at which the deflected feature disappears could not be determined but once it does, the vertical extent of the defects decreases and, with a diminishing of the pit, the surface becomes flat with no discernible defect remaining. A similar recovery is seen when the defect had not deflected, with first a reduction in the defect opening until it is seen edge-on, followed by a reduction in length with some remanent dark features whose identity could not be resolved. On reapplying a voltage, the morphological sequences are repeated and on subsequently voltage cycling the pits forming at the same locations. In reflected light, scar-like features can be seen at zero voltage where the defects had closed up, as has previously been noted [6]. This is most vividly seen from the video recordings, such as those presented in the Supplementary Materials.

4. Discussion

No theoretical or analytical model currently exists to describe the electric field induced surface morphological behavior beyond the initial surface perturbation instability to compare with our observations. So, in the absence of any model, the different stages in the evolution of the pre-breakdown defects with increasing

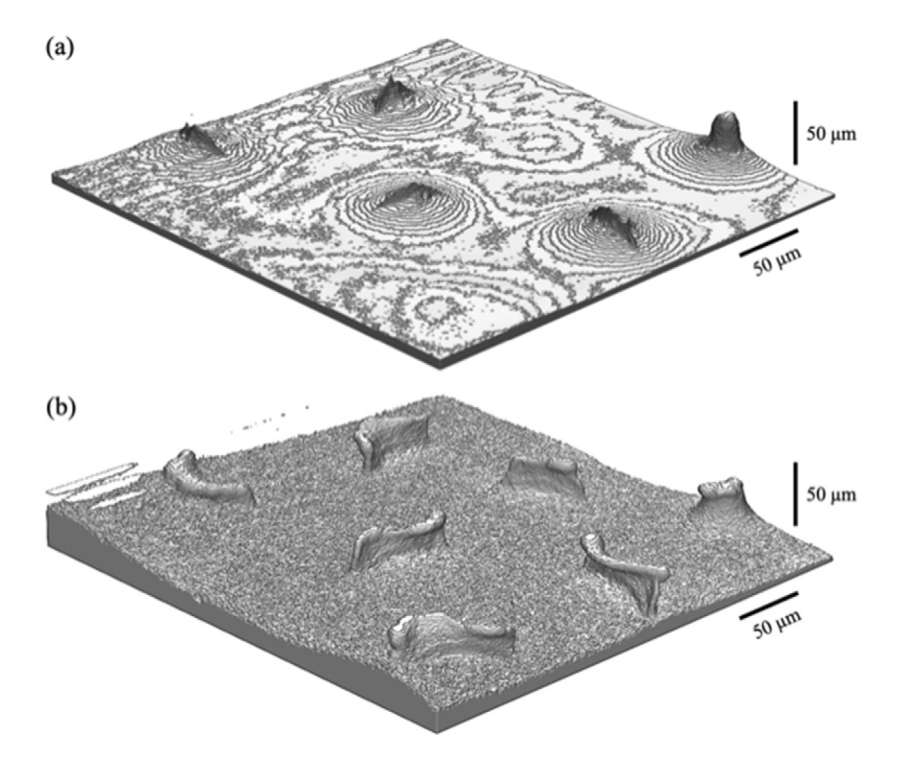


Fig. 4. Inverse height contours of the soft elastomer surface at 4.5 kV (top) and 5.5 kV (bottom) of the same region. As the voltage is increased, two new defects form, and the slit-like portions of the defects increase in height and some twist. The contours are spaced 0.91 μ m apart.

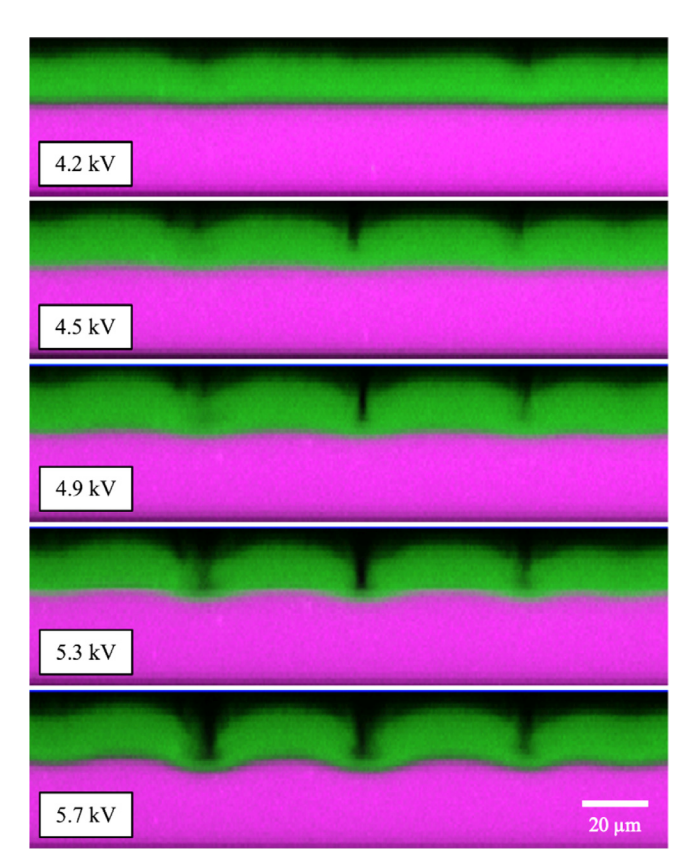


Fig. 5. Cross-sectional images of the defect evolution in a 15 μm soft elastomer on a stiff elastomer 30 μm at the successive voltages indicated.

electric field, in what we term the post-instability regime, are considered sequentially. We assume that the elastomer surface is conducting so that potential everywhere along the surface is the same although, of course, the charge density may not be. Initially, when a potential is applied through the thickness of the elastomer dielectric, the Coulombic attraction between the electric charges on the electrodes produce a compressive Maxwell stress in the field direction. As the elastomer bilayer is attached to the underlying ITO electrode both its mechanical displacement parallel and perpendicular at the electrode are fixed as is the electric displacement field at the ITO/elastomer interface. Further, as elastomers are almost perfectly incompressible materials, the electric field creates a hydrostatic compressive stress field [3] within the elastomer, given by:

$$\sigma_{11} = \sigma_{22} = \sigma_{33} = -\varepsilon \varepsilon_0 \left(V_0 / h \right)^2 / 2$$

where h is the elastomer thickness. As indicated, the magnitude increases quadratically with electric field. At the observed nucleation condition of \sim 3.8 kV, a field of \sim 50 V/micron, the hydrostatic compressive stress is calculated to be about 30 MPa. To put this stress in perspective, this compares with the shear modulus of the soft elastomer that is \sim 3 kPa.

The images suggest that at a higher electric field there is a second, abrupt shape transition from an axi-symmetric funnel shape to a slit-like, planar feature. This is seen particularly clearly in both the cross-section and from the surface contours plots, such as Fig. 4. This occurs at $\sim\!\!4$ kV (field of $\sim\!\!50$ V/micron). This shape transition is attributed to a geometrical collapse of the defects when the compressive stress field reaches a critical value where it is energetically favorable.

With increasing electric field, the defects extend deeper into the soft elastomer but do not change in their cross-sectional length (in the plane of the image slice). Their slit-like shape suggests that their shape is dominated by the compressive biaxial stress in the plane of the elastomer since, making an analogy with second-phase elastic inhomogeneities in a solid, the elastic strain energy density is a minimum for a high-aspect ratio oblate spheroid. The limited field of view of the confocal microscope

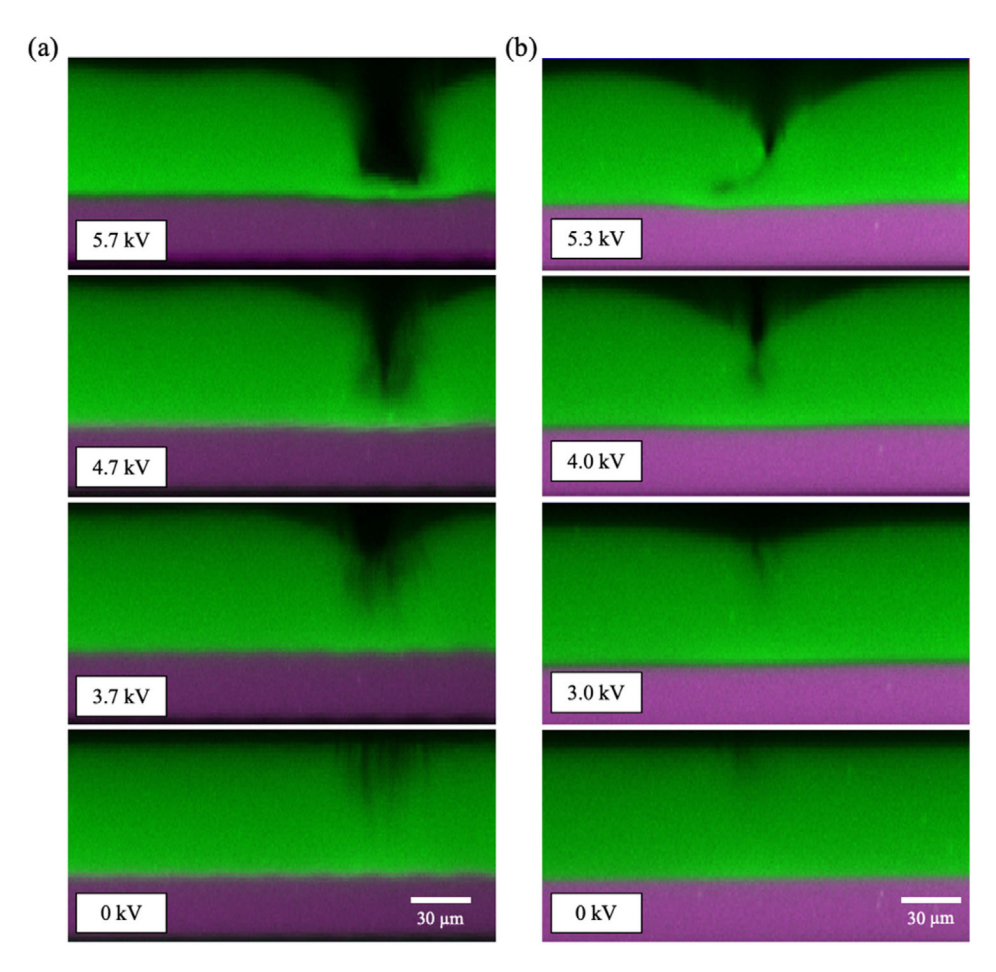


Fig. 6. Sequence of cross-section images recorded as the voltage is reduced back to zero from the maximum voltages indicated. (Left). Collapse of a columnar defect and (right) of a kinked defect. In both cases, the soft layer is 50 μm thick on a 30 μm stiff layer.

prevents imaging many defects simultaneously but no preferential alignment is apparent. With the imaging data obtained, including the apparent variation in defect thickness obtained by varying the contour threshold level, it is not possible to determine whether these defects have a finite or zero thickness, as might be expected with a crease where the two surfaces are in direct contact. However, as the surfaces are expected to be charged with the same sign of charge, it would be reasonable to expect that they must have a finite thickness determined by a balance between electrostatic repulsion between opposing charged surfaces and lowering the elastic strain energy associated with the defect being located in a compressive stress field. Without knowing how the charge redistributes along the defect surfaces with increasing voltage, the electrostatic repulsion cannot be estimated but the Coulombic repulsion is expected to vary inversely with the square of the distance between the charged parallel surfaces.

At still higher electric fields, the crack-like features begin to twist, in-plane. No explanation is proposed for this behavior, but it is noted that some of the images indicate that there is no preferential direction for the twisting to occur although the images suggest that they have a propensity to twisting in opposing directions, for instance in Fig. 2 (image 44). This is suggestive of minimizing any tetragonal elastic interactions between the defects. We note that as this change in geometric shape is occurring at very high electric fields, the spatial average of the hydrostatic stress field is expected to also be higher than that at which the initial instability occurs. These changes may be the result of local instabilities in response to gradients in elastic modulus as will be described later.

Then, at still higher fields the defects deflect away from the dielectric interface as they approach the interface, deforming the higher stiffness dielectric (purple) at the same time. This occurs at a field above about 5.4 kV (128 V/micron). The deflection behavior has, as far as we are aware, no precedent in either the mechanics of crack deflection in homogeneous brittle solids or creasing phenomena in very soft materials such as gels. (Crack deflection occurs in polycrystalline ceramics but this is associated with a preferential intergranular fracture associated with grain boundaries having a low fracture energy relative to the ceramic grains [15]. In the case of polycrystalline ceramics, the deflection is determined by the angle of a weaker grain boundary relative to the crack propagation direction). The possibility that the deflection we observe is due to electrostatic effects is considered unlikely since both the soft and stiff elastomers have very similar dielectric constants, consistent with the expectations of the liquid dielectric model and do not depend on the degree of crosslinking. In support of this conclusion, the dielectric constant of PDMS is, within measurement uncertainty, independent of the cross-linking ratio [16], and consequently there is no change in permittivity across the interface. There is, however, an almost two orders of magnitude difference in shear modulus across the interface. To investigate this, a series of experiments were performed with the same soft-elastomer but with stiff-elastomers having different cross-linking and hence elastic constants. Fig. 7.

Our observations suggest that the deflection is most probably due to elastic mismatch between the two elastomer layers with the defect remaining in the softer elastomer to minimize the overall strain energy density. Notably, the defects do not deflect

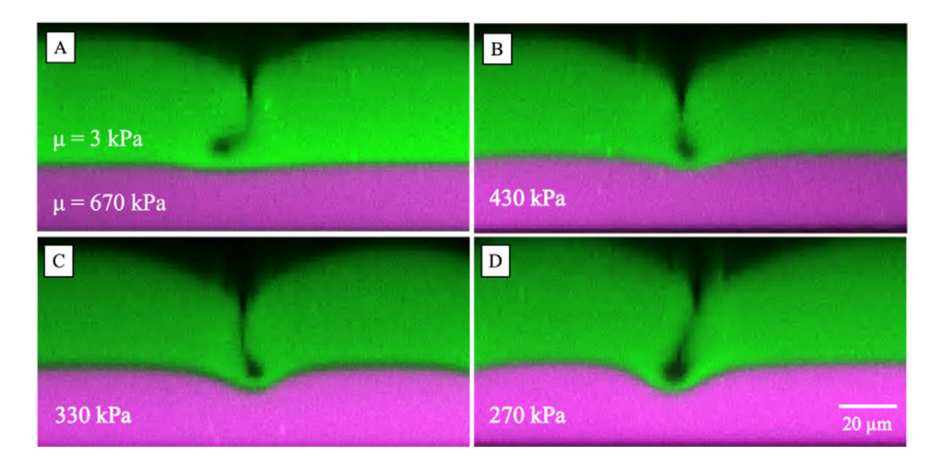


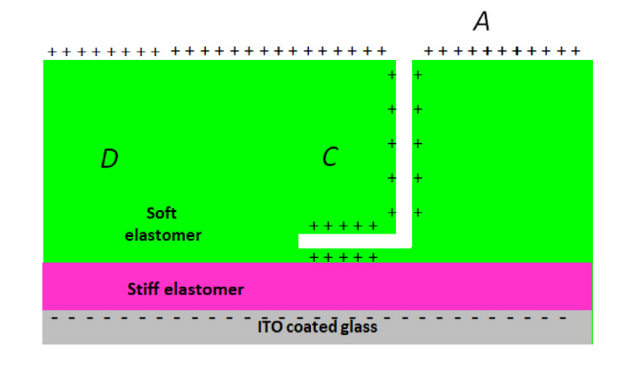
Fig. 7. Defects in the soft elastomer at similar stages in their evolution in samples having the same soft (50:1) elastomer layer on stiff layers having differing shear modulus (indicated) produced by altering the cross-linking ratio from 10:1 to 15:1 to 20:1 and to 25:1 cross-linking ratio. Applied voltage 5 kV.

in any preferred direction. This is also seen in the inverse, contour images illustrated in Fig. 4. Here we attribute the deflection to the existence of a gradient in the elastic modulus across the interface between the soft and stiff elastomers, possibly due to inter-diffusion between the elastomers on curing. The basis for assuming that the defect deflection is associated with a gradient in elastic modulus is that the deflection occurs well before the interface is reached and that the deflection trajectory is curved, as seen in Figs. 3 and 7, in all but the thinnest of soft layers (Fig. 5). For comparison, when a crack approaches an abrupt material interface, elastic mechanics predict that it propagates to the interface without deflecting and then either penetrates through the interface or deflects at the interface and runs along the interface [17].

The final evolutionary stages in which the defects open to become volume defects poses a conceptual problem as to how this can occur when the elastomer is notionally under a large hydrostatic compression from the Maxwell stress. It is further complicated because a wide variety of opening shapes are observed. Nevertheless, the final state resembles an array of holes, sometimes of quite irregular cross-section. It is proposed that this radical shape change must be associated with a local relief of the compressive stress field in the nominal applied electric field direction since it would otherwise keep the faces of the kinked defect closed. Two possibilities are suggested. The first is that, once deflected, the electrostatic repulsion of charges on the opposing faces, which are of the same sign as at the top surface, not only repel one another to open the defect but also decrease the local potential through the thickness of the soft elastomer, in the region, C. This, in turn, decreases the compressive stress acting locally. Well away from the defect, such as in region D, where the vertical component of the electric field is unchanged, the stress remains compressive. With further increases in voltage more charge is supplied increasing the charge density on opposing surfaces and the faces are forced further apart. Concurrently, the charge density on the vertical surfaces of the defect increase forcing them to also open.

The second, related possibility is that at sufficiently high fields when no deflection occurs, the local deformation in the stiff elastomer, visible in Fig. 5, causes the soft elastomer surface to no longer be planar reducing the compressive stress and the charge supplied to the faces of the defects becomes so large that the vertical faces repel and move apart.

Although we lack a detailed electro-mechanics analysis, our images suggest that the various intermediate stages evolve towards an equilibrium state, under high electric fields, consisting of an array of parallel, hyperbolic funnel shaped holes each



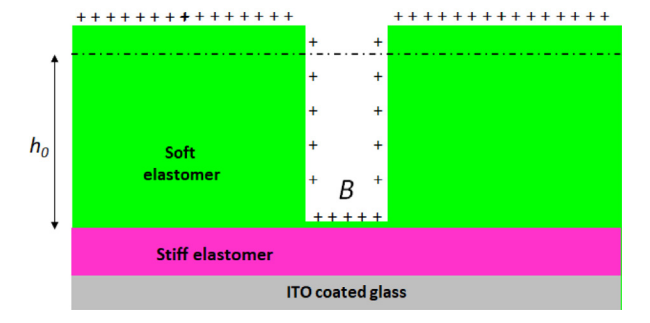


Fig. 8. (Top) Schematic of the charge distribution along the kinked defect indicating that the elastomer in regions, C, above the defect is under reduced electric field, and hence decreased compressive stress. (bottom) Schematic of the proposed equilibrium two-phase state consisting of holes extending almost down to the stiff elastomer and having a spacing corresponding to the spacing of the initial instability perturbations. The cylindrical shape is an idealization of what is believed to be a hyperbolic funnel shape that is required to satisfy the overall charge distribution. The uniform spatial charge distributions are likewise an idealization. The thickness of the elastomer before a voltage is applied is h_0 .

extending down almost through the full thickness of the soft elastomer. The spacing between the holes is set by the initial pit spacing, given by wavelength of the initial perturbation instability. To conserve the total elastomer volume, the formation of the holes requires that the thickness of the elastomer in between increases, decreasing the electric field in those regions, such as *A*, in the idealized axi-symmetric, volume element representation shown in Fig. 8 (b). This suggests a form of "two-phase" coexistence under field, one phase being circular, charged regions, *B*, arranged in a second phase consisting of the matrix of soft elastomer under a lower electric field. Assuming that everywhere

along the surface is at the same potential, the electric field in the area B is substantially higher than in regions A. For the bilayers considered in Figs. 2 and 3, the electric field in region B would be ~ 180 V/micron, based on the thickness of the stiff elastomer, whereas the approximate field in region A is ~ 60 V/micron. For comparison, the average, large-area, breakdown field of 10:1 Sylgard 184 is 130 V/micron [16]. This, in turn, suggests that the complex evolution in defect states are geometric paths by which an initial, uniform distribution of charge over the soft elastomer at low fields, prior to the surface instability, transitions to a two-phase state as the voltage and charge supplied increase.

Such a two-phase model suggests that there are four contributions to the total energy: (1) the overall elastic strain energy, (2) the electrostatic energy associated with the two geometric phases, each acting as an individual capacitor, (3) the electrical energy associated with the repulsion of electrostatic charges of the same sign on the surfaces of the tubes, and (4) the increase in surface energy with the formation of the tubes. (The surface energy of elastomers is of the order of 20 mJ/cm²). Although having a different origin, all the energy terms increase in magnitude with increasing voltage and charge density.

Once the two-phase state is reached, it is of interest to consider both the evolution when the applied voltage is further increased, as well as when the voltage is reduced back to the zero-voltage state. When the applied voltage is increased, more charge flows to the exposed surfaces of the holes, increasing the electrical energy. This results in an increase in the electric field at the bottom of the holes, as well as an increase in the radius of the holes, until catastrophic electric breakdown occurs at one of the many holes along the soft/stiff elastomer interface. One consequence is to alter the probability of electrical breakdown. Without the soft elastomer layer, the whole surface area of the stiff elastomer is at the same potential and electrical breakdown most likely occurs when the local electric field at some surface (or volume) defect exceeds the breakdown strength to form a single, or branched, filamentary breakdown that extends catastrophically through the stiff elastomer to the ITO electrode. However, with the soft elastomer layer in place, the regions of high electric field become localized by the initial surface instability to a considerably smaller proportion of the total area of the stiff elastomer with the commensurate decrease in probability of the local areas coinciding with defects on the surface of the stiffer elastomer. In essence, the lateral growth of the soft dielectric holes accompanying the growth of the defects allows the surface charge produced by the applied voltage to flow along the air/elastomer interface to patches of exposed interface of higher capacitance. Given that there will inevitably be some variability in the evolution of the defects, the area of exposed interface will vary spatially. Should the exposed area happen to coincide with a pre-existing defect in the stiff dielectric, then there is a high probability of breakdown occurring through the stiff dielectric but otherwise breakdown is delayed to a higher potential.

On the other hand, if catastrophic electrical breakdown does not occur and the applied voltage is reduced, removing charge, the identical sequence of defect shape changes does not have to occur in reverse although it appears to do so as seen in Fig. 6. Initially, the length of the holes will decrease, decreasing the thickness of the elastomer between the holes thereby increasing the compressive stress in the elastomer. At some voltage, the compressive stress will have increased until the holes collapse to form planar features that persist until the voltage is removed. Unless, the surfaces are perfectly clean, the faces of planar features will not perfectly match, and a permanent scar will remain. They may also be preferred sites for charge retention. Observations show that these then serve as preferred locations for the nucleation of pits when a voltage is again applied [6].

5. Concluding remarks

Once the electric field across the thickness of a soft, flat elastomer exceeds the initial bifurcation condition at which surface undulations grow, they undergo a series of complex morphological changes that are reversible when the voltage is removed. The evolution of each, described in this work as pre-breakdown defects, is slightly different in detail but they all transition from an approximately periodic array of axi-symmetric pits to closed "crack-like" features that propagate in the field direction until they open to form irregular shaped holes extending through the thickness of the elastomer. The abrupt transition from axi-symmetric pits to "crack-like" defects is attributed to the increasing compressive stress induced by the increasing electric field. Subsequently, the defects can open when the electric field no longer remains spatially uniform.

Our observations provide insight into possible mechanisms by which dielectric interfaces can be used to increase electrical breakdown strength. One of the strategies for preventing catastrophic electrical breakdown is to use a bi-layer dielectric as illustrated in this work. The common rationale, borne from practical experience, is that defect-nucleated breakdown in one layer will not propagate into the second layer since there is a low probability of a defect located in the second layer coinciding with the breakdown path in the first layer. Typically, this can occur when there is a pinhole in one layer, produced during processing for instance. A second strategy is incorporate platelets of a higher breakdown material to increase the breakdown strength. In this case, it has been proposed that the filamentary pre-breakdown defect deflects around the platelet, increasing the field necessary for catastrophic breakdown to occur through the total thickness of the dielectric. The mechanism by which the deflection occurs has not been described. The viability of this mechanism is supported by phase field modeling, performed in two-dimensions, of a stiff elastomer containing higher dielectric constant platelets aligned perpendicular to the nominal electric field [18]. Our work suggests that a gradient in elastic modulus provides a mechanism for the pre-breakdown defect to deflect before the dielectric interface is reached and that this can cause in an increase in breakdown field.

Declaration of competing interest

The authors declare that they have no known competing financial interests or personal relationships that could have appeared to influence the work reported in this paper.

Acknowledgments

We thank Professor Joanna Aizenberg for the use of the confocal microscope and to both Matthias Kollosche and Ehsan Hajiesmaili for invaluable discussions and assistance. This work was partially supported by the National Science Foundation, United States through the MRSEC Program (DMR 20-11754).

Appendix A. Supplementary data

Supplementary material related to this article can be found online at https://doi.org/10.1016/j.eml.2021.101473.

References

- [1] Q. Wang, L. Zhang, X. Zhao, Creasing to cratering instability in polymers under ultrahigh electric fields, Phys. Rev. Lett. 106 (2011) 118301.
- [2] E. Hajiesmaili, D.R. Clarke, Dielectric elastomer actuators, J. Appl. Phys. 129 (15) (2021) 151102.

- [3] J.W. Hutchinson, Surface instabilities of constrained elastomeric layers subject to electro-static stressing, J. Mech. Phys. Solids 153 (2021) 104462.
- [4] Z. Suo, Theory of dielectric elastomers, Acta Mech. Solida Sin. 23 (6) (2010) 549-578.
- [5] S. Shian, D.R. Clarke, Electrically-tunable surface deformation of a soft elastomer, Soft Matter 12 (2016) 3137.
- [6] S. Shian, P. Kjeer, D.R. Clarke, Electric-field induced surface instabilities of soft dielectrics and their effects on optical transmittance and scattering, J. Appl. Phys. 123 (2018) 113105. Q. Wang, X. Zhao, Creasing-Wrinkling transition in elastomer films under
- electric fields, Phys. Rev. E 88 (2013) 042403.
- Q. Wang, X. Zhao, Beyond wrinkles: Multimodal surface instabilities for multifunctional patterning, MRS Bull. 41 (2016) 115-122.
- S. Shian, D.R. Clarke, Electrically tunable window devices, Opt. Lett. 41 (6) (2016) 1289-1292.
- [10] I.D. Johnston, et al., Mechanical characterization of bulk Sylgard 184 for microfluidics and microengineering, J. Micromech. Microeng. 24 (3) (2014).

- [11] R.N. Palchesko, et al., Development of polydimethylsiloxane substrates with tunable elastic modulus to study cell mechanobiology in muscle and nerve, PLoS One 7 (2012) e51499.
- F. Schneider, et al., Mechanical properties of silicones for MEMS, J. Micromech. Microeng. 18 (6) (2008).
- [13] E. Hajiesmaili, Voltage-Induced Pitting Pattern of Constrained Dielectric Elastomer Membranes, 2018.
- [14] P. Chareon-Rajapark, D.R. Clarke, Unpublished work (2020).
- [15] D.R. Clarke, K.T. Faber, Fracture of ceramics and glasses, J. Phys. Chem. Solids 48 (11) (1987) 1115-1157.
- [16] M. Kollosche, Dielectric properties of elastomers, Private Commun. (2020).
- [17] M.Y. He, J.W. Hutchinson, Crack deflection at an interface between dissimilar elastic materials, Int. J. Solids Struct. 25 (1989) 1053-1067.
- [18] K.C. Pitike, W. Hong, Phase-field model for dielectric breakdown in solids, J. Appl. Phys. 115 (2014) 044101.